Fast particles overtaking shock front in two-dimensional Yukawa solids

Pengwei Qiu and Yan Feng ◉*

Institute of Plasma Physics and Technology, School of Physical Science and Technology, Soochow University, Suzhou 215006, China

High-speed particles overtaking the shock front during the propagation of compressional shocks in two-dimensional (2D) Yukawa solids are investigated using molecular dynamical simulations. When the compressional speed is lower, all particles around the shock front are almost accelerated synchronously. However, when the compressional speed is much higher, some particles penetrate the shock front to enter the preshock region. Around the shock front, it is found that the particle velocity profile at the first peak of the dispersive shock wave (DSW) is able to be described using the Gaussian distribution, so that the amplitudes of the DSW can be well characterized. As the compressional speed increases, the particle velocity corresponding to these DSW's amplitudes increase more substantially than the shock front speed. These amplitudes of the DSW are found to be able to predict the occurrence of the fast particles. Combined with the previous study of the DSW's period, it is demonstrated that the properties of the DSW are nearly not affected by the conditions of the 2D Yukawa systems, but only related to the compressional speed.

I. INTRODUCTION

A dispersive shock wave (DSW) exhibits the periodic structure, consisting of a series of envelopes with the monotonically decreasing amplitudes [1], where the dispersive effect is much greater than the dissipative one [2]. The DSWs have been investigated in various physical systems, such as the nonlinear optics [3,4], fluids [5–7], the Bose-Einstein condensates [8,9], and dusty plasmas [10–13]. DSWs typically occur where the weak dispersion and weak nonlinearity are dominant [14].

Laboratory dusty plasma typically refers to the mixture of free electrons, free ions, neutral gas atoms, and charged micron-sized dust particles [15–28]. Because of their high charge Q and low charge-to-mass ratio, these dust particles are strongly coupled, so that the collection of thousands of dust particles typically exhibits the properties of either liquids [29–32] or solids [33–36]. In the typical laboratory conditions, tens of thousands of dust particles can be suspended in the plasma sheath, forming a two-dimensional (2D) suspension, i.e., a 2D dusty plasma [22,23,37]. Due to the low frictional gas drag [38], the motion of these dust particles in the plasma is underdamped. The interaction between particles can be modeled as the Yukawa repulsion [39–41]. The motion of individual dust particles within this 2D plane can be directly recorded using video imaging, so that the diagnostic of individual particle tracking can be employed [42]. Now, dusty plasma has been developed to an excellent model system, in which various fundamental physics processes can be investigated at the kinetic level [43]. Quite a few shock-related experiments have been performed in dusty plasmas, such as the mach cones generated by supersonic particles [44], the

shock melting generated by an electric pulse [45], and the compressional shock generated by a moving exciter [46].

Using computer simulations of dusty plasmas, more quantitative analyses can be accurately performed to investigate properties of compressional shocks [10–13,47–50]. In Ref. [10], compressional shocks are generated by a inward moving boundary in 2D Yukawa systems, so that the thermodynamic and kinetic properties are obtained. In Refs. [11,12], from the shock Hugoniot curve, thermodynamic quantities of the pressure and energy in the postshock region are analytically derived. The presence of fast particles ahead of the shock front is revealed from these simulations [10,11]. In fact, these fast particles have also been observed in the shock wave propagation in the three-dimensional (3D) dusty plasma experiment performed on the international space station [51]. However, from our literature search, the underlying mechanism of these fast particles has still not been well understood yet. Under some conditions, the DSW has been observed around the shock front of compressional shocks [10], which is further confirmed in Refs. [11–13]. In Ref. [13], it is found that the DSW's period is almost only related to the compressional speed of the boundary, nearly independent from the conditions of 2D Yukawa systems. However, the property of the DSW's amplitude in this system is still unknown yet. Here, we explore the mechanism of the DSW's amplitude, and also look for the connection between the DSW's amplitude and the so-called fast particles.

In this paper, we study the high-speed particles which overtake the shock front during the propagation of compressional shocks in 2D Yukawa solids using molecular dynamical (MD) simulations. In Sec. II, we briefly introduce our MD simulation method to mimic compressional shocks in 2D Yukawa solids. In Sec. III, we investigate the DSW by characterizing its amplitude under various conditions. Then, comparing the obtained DSW's amplitude with the shock front speed derived

---

*fengyan@suda.edu.cn

from the shock Hugoniot curves, we provide our interpretation of the fast particles around the shock front and also predict the occurrence of these fast particles under various conditions. Finally, a summary is given in Sec. IV.

II. SIMULATION METHOD

To mimic dynamics of compressional shocks in 2D dusty plasmas, we perform MD simulations of 2D Yukawa systems using LAMMPS [52] as in Refs. [11–13,47–50]. The simulated $N = 16\,384$ particles are confined in a 2D plane with the initial size of $486.6a_0 \times 105.6a_0$, where a_0 is the Wigner-Seitz radius of the initial undisturbed 2D Yukawa system. The interaction between particles is the Yukawa repulsion $\phi_{ij} = Q^2 \exp(-r_{ij}/\lambda_D)/4\pi\epsilon_0 r_{ij}$, where λ_D is the Debye length, Q is the particle charge, and r_{ij} is the distance between the particles i and j. To describe our 2D Yukawa system, two dimensionless quantities are used, which are the coupling parameter $\Gamma_0 = Q^2/(4\pi\epsilon_0 a_0 k_B T)$ and the screening parameter $\kappa_0 = a_0/\lambda_D$, respectively, where T is the kinetic temperature of particles. The initial coupling parameter is always specified as $\Gamma_0 = 2000$ for all 2D Yukawa solids studied here. Note that we use the symbols with the subscript 0 to represent the physical quantities of the undisturbed preshock region, as in Refs. [11,12].

Besides the interparticle interaction, in the x direction, two inward confining forces from the left and right boundaries are also applied in our simulations, respectively. Here, the magnitude of the confining force is $F_i = 50 \exp[-(x - x_b)^2/0.25a_0^2]ma_0\omega_{pd}^2$, where x_b refers to the location of the boundary, and ω_{pd} is the nominal 2D dusty plasma frequency [53,54]. To generate compressional shocks generated in a 2D Yukawa solid, the left boundary is specified to move to the right with various constant speeds of v_{left}, while the right boundary is stationary. In the y direction, the periodic boundary conditions are applied. Other details of our MD simulation method are the same as in Ref. [50]. After obtaining the positions and velocities of the simulated 16 384 particles, we are able to perform the corresponding data analysis, as presented next.

III. RESULTS AND DISCUSSION

To study the particle motion around the shock front during the shock propagation, we prepare the typical particle trajectories with two different compressional speeds of $v_{left}/a_0\omega_{pd} = 0.636$ and 1.061 in Fig. 1. Here, we plot the trajectories of particles around the shock front within the region of $50a_0 \times 40a_0$, nearly 4% of the entire simulation box, when $113 \leqslant t\omega_{pd} \leqslant 127$ after the left boundary starts to compress the 2D Yukawa solid. Note that the initial conditions of our simulated 2D Yukawa solid in Fig. 1 are $\Gamma_0 = 2000$ and $\kappa_0 = 0.75$.

Figure 1 clearly shows two different types of particle motion around the shock front during the propagation of compressional shocks. After the left boundary starts to compress the 2D Yukawa solid, particles in the postshock region are accelerated significantly by the generated shock. For the lower compressional speed in Fig. 1(a), all particles at the shock front are almost accelerated synchronously, and the shock front speed is higher than the speed of the particle motion.
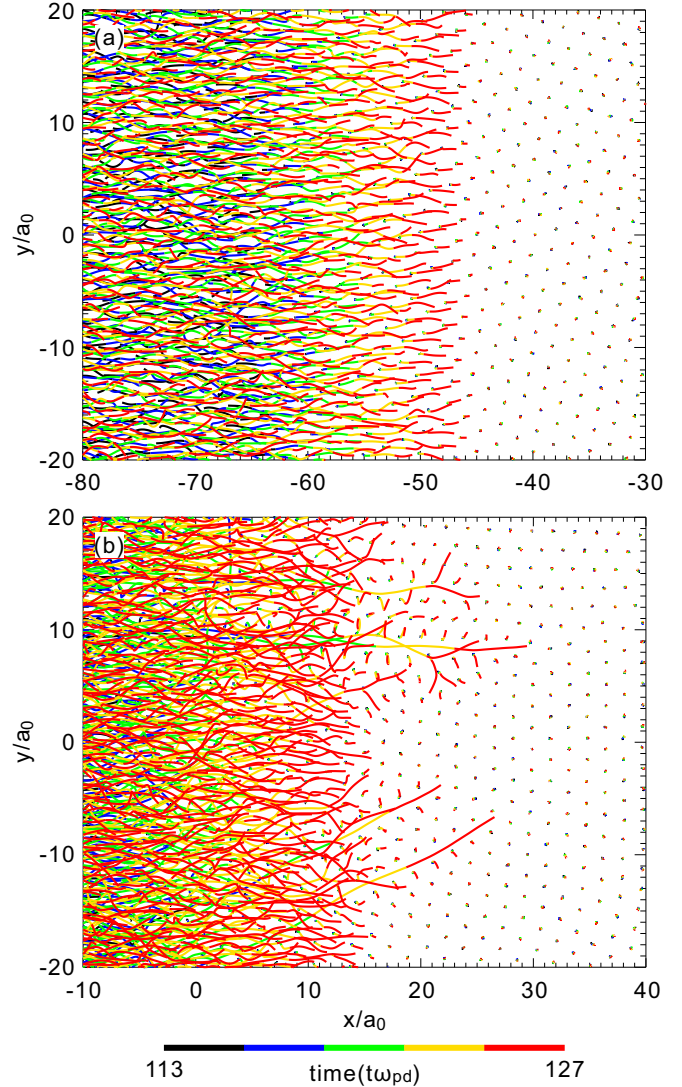
FIG. 1. Calculated particle trajectories around the shock front for the compressional speeds of (a) $v_{left}/a_0\omega_{pd} = 0.636$ and (b) 1.061 in the 2D Yukawa solid of $\Gamma_0 = 2000$ and $\kappa_0 = 0.75$. Clearly, the collective motion of particles around the shock front exhibits two different behaviors during the propagation of compressional shocks. For the higher compressional speed of $v_{left}/a_0\omega_{pd} = 1.061$ in panel (b), a few particles penetrate the shock front and then enter the preshock region. However, for the lower compressional speed of $v_{left}/a_0\omega_{pd} = 0.636$ in panel (a), the motion of all particles around the shock front is almost synchronized, so that none of them penetrate the shock front to enter the preshock region. Note that only 4% of the simulated region and 3% of the simulated duration are shown here.

However, from Fig. 1(b), when the compressional speed is higher, a few of particles penetrate the shock front and then enter the preshock region. In this paper, we follow the tradition of Ref. [10] to name these particles overtaking the shock front as "fast particles." In fact, these fast particles have also been observed in the previous shock simulations [10,11], while the detailed investigation is still lacking.

To effectively quantify these fast particles around the shock front, we prepare the one-particle distribution function

$f_1(\zeta, v_x)$, as in Refs. [10–13]. Here, ζ is the Lagrange coordinate $\zeta = x - (Dt - 240)$ moving with the shock front, where D is the shock front speed derived from the shock Hugoniot curve [11]. First, we divide the $\zeta - v_x$ plane into bins in the both ζ and v_x directions. For the horizontal axis of ζ, we divide it into bins with the width of $0.5a_0$. While for the vertical axis of v_x, we divide it into bins with the width of $0.01a_0\omega_{\text{pd}}$. Then we count the particle number in each cell, and divide it by the total particle number in all cells to obtain the distribution function, as shown in Figs. 2(a) and 2(c). Besides the distribution function, we also calculate the corresponding velocity profiles at the first peak of the DSW, as shown in Figs. 2(b) and 2(d), respectively. The velocity profile provides the distribution of the particle velocity v_x at the first peak of the DSW with the width of $1.0a_0$. Note that the initial conditions of Figs. 2(a) and 2(c) are the same as those of Figs. 1(a) and 1(b), respectively.

In fact, while preparing Fig. 2, the shock front speed D in the Lagrange coordinate ζ is derived from the shock Hugoniot curve obtained from the initial conditions of $\Gamma_0 = 800$ in Ref. [11]. The initial coupling parameter of our studied Yukawa solids here is $\Gamma_0 = 2000$, with 40% of the kinetic temperature of $\Gamma_0 = 800$ in Ref. [11]. However, from the test runs of our simulations, we confirm that, for compressional shocks in 2D Yukawa systems of $\Gamma_0 = 800$ and $\Gamma_0 = 2000$, the resulting shock front speeds are almost exactly the same. Thus, in Fig. 2, as well as in Figs. 3 and 4 reported later, we still use the shock Hugoniot curves in Ref. [11] to derive the shock front speed D.

The amplitude of the DSW can be easily obtained from the obtained one-particle distribution function $f_1(\zeta, v_x)$ and the corresponding velocity profiles. From Figs. 2(a) and 2(c), a few ripples can be observed around the shock front region, just corresponding to the structure of the DSW. We find that the velocity profiles of v_x at the first peak of the DSW in Figs. 2(b) and 2(d) can be well described using the Gaussian distribution of

$$f(x) = e^{-\frac{(x-\mu)^2}{2\sigma^2}} \big/ \sigma\sqrt{2\pi}, \tag{1}$$

as the fitting curves shown in Figs. 2(b) and 2(d). Thus, the fitting parameter of σ can be used to characterize the magnitude of the DSW quite well. Clearly, μ is the averaged drift velocity of particles at the location of $\zeta = 0$, while σ the width of the Gaussian profile there. For the Gaussian distribution, the particle velocity probabilities of $\geqslant \mu + 2\sigma$ and $\geqslant \mu + 3\sigma$ correspond to 2.3% and 0.13%, respectively. Since for the Gaussian distribution, the probability of $\geqslant \mu + 4\sigma$ is very tiny, we ignore it for our current investigation. As a result, we are able to use the thresholds of 2σ or 3σ to characterize the magnitude of the DSW, which here we term as the amplitude of the DSW. These two amplitudes of the DSW essentially represent the drift velocity of some fast particles faster than $\mu + 2\sigma$ and $\mu + 3\sigma$ along the shock propagation direction around the shock front. We plot the velocities of $\mu + 2\sigma$ and $\mu + 3\sigma$ corresponding to the DSW's amplitudes, along with the shock front speed D in Figs. 2(a) and 2(c) for the intuitive comparison.

From Fig. 2, we can easily observe the relationship between the particle velocities corresponding to the DSW's amplitudes of 2σ, 3σ and the shock front speed D. For the
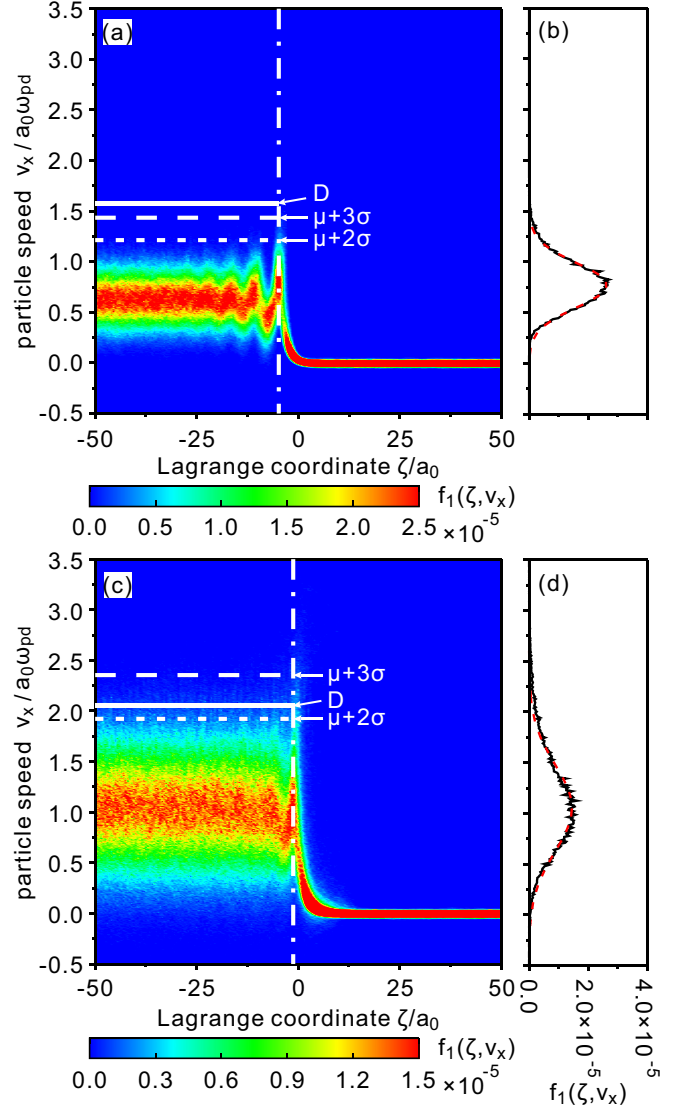
FIG. 2. Obtained one-particle distribution function of the particle velocity $f_1(\zeta, v_x)$ for the compressional speed of (a) $v_{\text{left}}/a_0\omega_{\text{pd}} = 0.636$ and (c) 1.061, as well as the corresponding velocity profiles in panels (b) and (d) at the first peak of the DSW, respectively. Clearly, the velocity profiles in panels (b) and (d) can be well described using the Gaussian distribution of Eq. (1), as the smooth dashed curves shown. Here, we name 2σ or 3σ as the DSW's amplitude, and mark the particle velocities corresponding to these DSW's amplitudes as $\mu + 2\sigma$ and $\mu + 3\sigma$ in panels (a) and (c). We also mark the corresponding shock front speed D [11] in panels (a) and (c) for the easier comparison. In panel (c), $\mu + 2\sigma < D$, while $\mu + 3\sigma > D$, indicating that some particles move faster than the shock front, well agreeing with Fig. 1(b) where some particles penetrate the shock front. However, in panel (a), $\mu + 2\sigma$ and $\mu + 3\sigma$ are both lower than D, well consistent with Fig. 1(a) where no particles penetrates the shock front. Note here the initial conditions of the 2D Yukawa solid are $\Gamma_0 = 2000$ and $\kappa_0 = 0.75$.

lower compressional speed in Fig. 2(a), both $\mu + 2\sigma$ and $\mu + 3\sigma$ are lower than the shock front speed D. However, for the higher compressional speed in Fig. 2(c), although $\mu + 2\sigma$ is still lower than the shock front speed D, $\mu + 3\sigma$ is
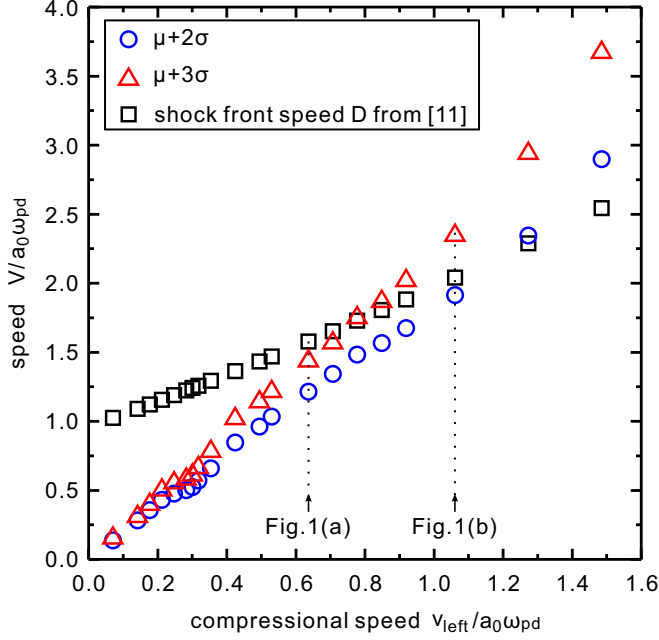
FIG. 3. Obtained particle velocities corresponding to these DSW's amplitudes of $\mu + 2\sigma$ and $\mu + 3\sigma$, as the functions of the compressional speed varying from $0.071a_0\omega_{pd}$ to $1.485a_0\omega_{pd}$, with the initial 2D Yukawa conditions of $\Gamma_0 = 2000$ and $\kappa_0 = 0.75$. For comparison, we also present the shock front speed D derived from the shock Hugoniot curve [11] for different compressional speeds. Clearly, as the compressional speed of the left boundary v_{left} increases, the shock front speed D increases simultaneously, and the particle velocities corresponding to these DSW amplitudes $\mu + 2\sigma$ and $\mu + 3\sigma$ also increase significantly and even more substantially. When the particle velocity corresponding to the DSW's amplitude eventually exceeds the shock front speed D, the corresponding percentage particles are able to penetrate the shock front to enter the preshock region, as those shown in Fig. 1(b). Note that the arrows shown here correspond to the conditions of Fig. 1.

significantly higher than the shock front speed D. The result of $\mu + 3\sigma > D$ in Fig. 2(c) clearly indicates that some particles move faster than the shock front speed, well agreeing with the observed fast particles in Fig. 1(b).

Note that although the velocity profiles in Figs. 2(b) and 2(d) can be fit to the Gaussian function quite well, they represent the particle drift velocity along the shock propagation direction. Due to the acceleration of the compressional shocks on all particles to the right in our simulations, the probability of the velocity distribution within the range of $(\mu, +\infty)$ is slightly higher than that within the range of $(-\infty, \mu)$, i.e., the calculated velocity profile is not strictly symmetric about $v_x = \mu$. However, our use of $\mu + 2\sigma$ or $\mu + 3\sigma$ to quantify the amplitude of DSW is still not affected much.

To understand the physical mechanism of fast particles around the shock front, we investigate the variation of the particle velocities corresponding to the DSW's amplitudes as the function of the compressional speed. By fitting the velocity profiles at the shock front using the method described above, we obtain the particle velocities of $\mu + 2\sigma$ and $\mu + 3\sigma$ corresponding to the two DSW's amplitudes for all compressional speeds, as presented in Fig. 3. For the comparison, we
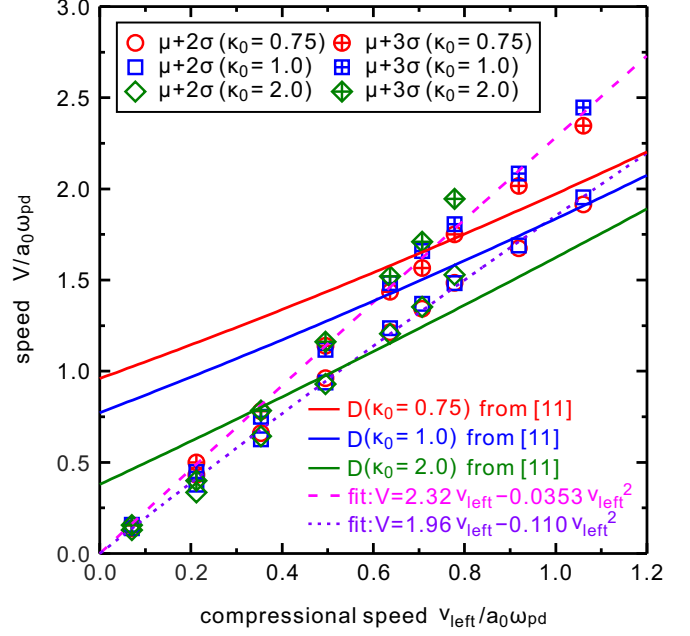
FIG. 4. Obtained particle velocities corresponding to the DSW's amplitudes $\mu + 2\sigma$ and $\mu + 3\sigma$, as the functions of the compressional speed v_{left}, under the conditions of $\kappa_0 = 0.75$, 1.0, and 2.0, while $\Gamma_0 = 2000$ for the initial 2D Yukawa solids. For the comparison, we also present the shock Hugoniot curves [11], i.e., the $D - \bar{v}$ relationship of 2D Yukawa system, where $\bar{v}$ is the same as the compressional speed v_{left} here [11], as the solid curves shown. Clearly, the obtained particle velocities corresponding to the DSW's amplitudes of $\mu + 2\sigma$ and $\mu + 3\sigma$ follow the same monotonically increasing trend with the compressional speed v_{left}. For these three κ_0 values, the obtained data points of $\mu + 2\sigma$ and $\mu + 3\sigma$ only scatter briefly, suggesting that the amplitude of the DSW is mainly determined by the compressional speed v_{left}, nearly not related to the initial screening parameter of the 2D Yukawa solids. The parabolic expression of $V = \alpha v_{\text{left}} + \beta v_{\text{left}}^2$ is used to fit to these symbols, as two dashed curves show. For the same compressional speed of v_{left}, although the obtained results of $\mu + 2\sigma$ and $\mu + 3\sigma$ for different κ_0 values are very close, the shock front speed D determined by the shock Hugoniot curves are completely different. From the crossings of the shock Hugoniot curves and the parabolic fittings of $\mu + 2\sigma$ and $\mu + 3\sigma$, the fast particles overtaking the shock front can be well predicted and characterized. Note when the compressional speeds $v_{\text{left}} = 0.919$ and 1.061 for $\kappa_0 = 2.0$, the DSW fades away so that the amplitude cannot be distinguished any more.

also present the corresponding shock front speed D calculated from the shock Hugoniot curve in Ref. [11]. Clearly, in Fig. 3, the shock front speed D is nearly linear to the compressional speed v_{left} [11], well agreeing with the theory of both viscous and dispersive shocks [55]. Note, in Fig. 3, the initial conditions of our 2D Yukawa solid are $\Gamma_0 = 2000$ and $\kappa_0 = 0.75$.

In Fig. 3, clearly, as the compressional speed increases, both the shock front speed D and the particle velocities corresponding to the DSW's amplitudes increase monotonically. However, the velocities corresponding to the DSW's amplitudes of $\mu + 2\sigma$ and $\mu + 3\sigma$ increase much more substantially than the shock front speed D. For lower compressional speeds of v_{left}, the particle velocities corresponding to

the DSW's amplitudes of $\mu + 2\sigma$ and $\mu + 3\sigma$ are both lower than the shock front speed D. For our studied 2D Yukawa solid of $\Gamma_0 = 2000$ and $\kappa_0 = 0.75$, when the compressional speed $v_{\text{left}}/a_0\omega_{\text{pd}} \gtrsim 0.8$, the particle velocity corresponding to the DSW's amplitude of $\mu + 3\sigma$ first exceeds the shock front speed D, we observe a few particles penetrate the shock front to enter the preshock region with a limited depth. When the velocity corresponding to the DSW's amplitude of $\mu + 2\sigma$ is comparable to or even higher than the shock front speed D, as in Fig. 1(b) of $v_{\text{left}}/a_0\omega_{\text{pd}} = 1.061$, we find that more particles penetrate the shock front and then enter sufficiently deep into the preshock region. As the compressional speed v_{left} increases further, more and more particles penetrate the shock front and enter the preshock region even deeper.

From Fig. 3, we also find that, as the compressional speed increases, the gap between $\mu + 2\sigma$ and $\mu + 3\sigma$ gradually increases. This result is reasonable, since the difference between $\mu + 2\sigma$ and $\mu + 3\sigma$ is just σ, which means the width of the velocity profile or the thermal velocity [12]. For the higher compressional speed, particles are more substantially accelerated, so that more energy from the compression is converted to the thermal energy around the shock front, i.e., the obtained velocity profile in Fig. 2 is wider.

As the major result of this paper, we find the relationship between the particle velocities corresponding to the DSW's amplitudes and the compressional speed v_{left} from our simulated 2D Yukawa solids under various conditions, as shown in Fig. 4. In addition to the results for $\kappa_0 = 0.75$ in Fig. 3, we also present the obtained particle velocities corresponding to the DSW's amplitudes for the other values of $\kappa_0 = 1.0$ and 2.0 in Fig. 4. Note that we confirm that the initial states of the simulated 2D Yukawa systems under these conditions of these κ_0 values and $\Gamma_0 = 2000$ are all solids [56]. Following the method described above, we obtain the particle velocities corresponding to the DSW's amplitudes of $\mu + 2\sigma$ and $\mu + 3\sigma$ for each pair of Γ_0 and κ_0, as shown in Fig. 4. We also present the shock Hugoniot curves derived in Ref. [11] for different κ_0 values, as the solid curves shown in Fig. 4, where the mean particle speed $\bar{v}$ is replaced by the compressional speed v_{left}, as confirmed in Ref. [11].

Interestingly, from Fig. 4, we find that when the initial screening parameter varies, the particle velocities corresponding to the DSW's amplitudes of $\mu + 2\sigma$ and $\mu + 3\sigma$ do not vary substantially. Unlike the shock front speeds D for various κ_0 values which are completely different, our obtained particle velocities of $\mu + 2\sigma$ and $\mu + 3\sigma$ only scatter very briefly for the different κ_0 values. That is to say, the particle velocities corresponding to the DSW's amplitudes are nearly not affected by the initial screening parameter κ_0 of the 2D Yukawa solids, well agreeing with the analytical predictions for weak DSWs [55,57,58]. Besides the DSW's amplitude presented here, in Ref. [13], it is also found that the period of the DSW is mainly determined by the compressional speed of the boundary, which is nearly independent from the initial conditions of 2D Yukawa systems, no matter how Γ_0 and κ_0 vary. Combining the results here and those in Ref. [13], it seems that the properties of the DSW, such as its amplitude and period, are almost only related to the compressional speed, and nearly independent from the conditions of the media where the shock

propagates, such as 2D Yukawa solids studied here or those studied in Ref. [13].

To better characterize the relationship between the particle velocities corresponding to the DSW's amplitudes and the compressional speed, we use the parabolic expression of

$$V = \alpha v_{\text{left}} + \beta v_{\text{left}}^2 \qquad (2)$$

to quantitatively describe these physical quantities instead of relying on discrete data points, as shown by two dashed curves in Fig. 4. Our chosen expression of Eq. (2) implies that the particle velocity corresponding to the DSW's amplitude is zero when the compressional speed v_{left} is zero, as we discuss later. The corresponding fitting coefficients of α and β in the parabolic expression are presented in the legend of Fig. 4. To keep the same weighting of data points for different κ_0 values, we only choose nine data points of $\kappa_0 = 0.75$ from Fig. 3, as presented in Fig. 4. However, all data points for $\kappa_0 = 0.75$ in Fig. 3 well agree with the presented fitting curves in Fig. 4. Note that when the compressional speed $v_{\text{left}} = 0.919$ and 1.061 for $\kappa_0 = 2.0$, the DSW almost vanishes so that the amplitude cannot be identified any more, and the similar feature is also observed in Ref. [13]. As a result, in Fig. 4, we only have seven data points for $\kappa_0 = 2.0$, unlike the nine data points for $\kappa_0 = 0.75$ or 1.0, for the parabolic fittings. Clearly, from Fig. 4, the ratio of the DSW's amplitude (such as $\mu + 2\sigma$) to the postshock drift velocity (just the compressional speed v_{left} [11]) is around 1.5, well agreeing with the theoretically predicted ratio [55,57,58] of about 1.5 to 2 for DSWs when the dispersive effect is dominant, as in Fig. 5 of Ref. [55].

From Fig. 4, we find that the obtained fitting curves intersect with the shock Hugoniot curves with different κ_0 values. Although our fitting curves of $\mu + 2\sigma$ and $\mu + 3\sigma$ both start from the initial point, they increase much more substantially than the shock Hugoniot curves, as the compressional speed increases. As a result, the particle velocities corresponding to the amplitudes of the DSW $\mu + 2\sigma$ and $\mu + 3\sigma$ characterized by the fitting curves gradually exceed the shock front speed D when the compressional speed v_{left} is between $0.5a_0\omega_{\text{pd}}$ and $1.0a_0\omega_{\text{pd}}$ for different κ_0 values. Essentially, when the particle velocity corresponding to the DSW's amplitude exceeds the shock front speed, the corresponding percentage particles move faster than the shock front. As a result, these particles overtake the shock front and then enter the preshock region. Thus, we are able to effectively predict the occurrence of the fast particles overtaking the shock front based on the crossings of the shock Hugoniot curves and the parabolic fittings of $\mu + 2\sigma$ and $\mu + 3\sigma$ in Fig. 4.

Note that, unlike the intercept of the shock Hugoniot curves indicates the corresponding longitudinal sound speeds of the undisturbed 2D Yukawa system [11], the particle velocity corresponding to the DSW's amplitude is always zero when the compressional speed of v_{left} is close to zero. When v_{left} is close to zero, the particles are barely accelerated, thus the drift velocity of particles, or the particle velocity corresponding to the DSW's amplitude, is almost zero, leading to our choice of the fitting equation (2) above.

From our compressional shock simulation results presented above, we provide our interpretation of the fast particles overtaking the shock front. When the compressional speed of the left boundary increases, both the particle

velocity corresponding to the DSW's amplitude and the shock front speed increase monotonically, while the particle velocity corresponding to the DSW's amplitude increases much more substantially than the shock front speed. If the particle velocity corresponding to the DSW's amplitude is comparable to or even higher than the shock front speed, i.e., some particles move faster than the shock front, then these fast particles are able to penetrate the shock front, just as in Fig. 1(b). Combining the quantitative relationship between the particle velocity corresponding to the DSW's amplitude and the compressional speed in Fig. 4 with the shock Hugoniot curves in Ref. [11], the fast particles occurring around the shock front during the shock propagation in 2D Yukawa solids can be well predicted.

IV. SUMMARY

In summary, we systematically investigated the fast particles overtaking the shock front during the propagation of compressional shocks in 2D Yukawa solids using MD simulations. From the obtained particle trajectories, we observe two different types of particle motion around the shock front during the propagation of compressional shocks. For the initial 2D Yukawa solid of $\Gamma_0 = 2000$ and $\kappa_0 = 0.75$, when the compressional speed $v_{\text{left}}/a_0\omega_{\text{pd}} \gtrsim 0.8$, we find some particles penetrate the shock front and then enter the preshock region. Applying the Gaussian fitting to the velocity profile of the one-particle distribution function, we obtain the amplitude of the generated DSW around the shock front which can be used to characterize these fast particles. The particle velocity corresponding to the DSW's amplitude and the shock front speed both increase monotonically with the compressional speed, however, the increase of the particle velocity corresponding to the DSW's amplitude is much more substantial. When the particle velocity corresponding to the DSW's amplitude increases to comparable to or even higher than the shock front speed, i.e., the shock propagation speed, the fast particles appear reasonably. We also find that the particle velocity corresponding to the DSW's amplitude under various conditions can be well fit by the parabolic expressions. Comparing these parabolic fittings of the velocity of the DSW's amplitudes with the shock Hugoniot curves, the occurrence of the fast particles during the shock propagation in 2D Yukawa solids can be well predicted and characterized under various conditions.

As for the property of the DSW in our simulations, we find that the initial screening parameter of 2D Yukawa solids nearly does not have an effect on our obtained amplitude of the DSW. Combined with the previous study on the period of the DSW [13], it seems that the properties of the DSW are nearly not related to the initial conditions of the media where the compressional shock propagates, but only related to the shock parameter of the compressional speed.

ACKNOWLEDGMENTS

[1] M. D. Maiden, N. K. Lowman, D. V. Anderson, M. E. Schubert, and M. A. Hoefer, Phys. Rev. Lett. **116**, 174501 (2016).

[2] Y. Matsuno, V. S. Shchesnovich, A. M. Kamchatnov, and R. A. Kraenkel, Phys. Rev. E **75**, 016307 (2007).

[3] C. Conti, A. Fratalocchi, M. Peccianti, G. Ruocco, and S. Trillo, Phys. Rev. Lett. **102**, 083902 (2009).

[4] M. Isoard, A. M. Kamchatnov, and N. Pavloff, Phys. Rev. A **99**, 053819 (2019).

[5] N. F. Smyth and P. E. Holloway, J. Phys. Oceanogr. **18**, 947 (1988).

[6] J. Lighthill, *Waves in Fluids* (Cambridge University Press, Cambridge, 1978).

[7] S. Trillo, M. Klein, G. F. Clauss, and M. Onorato, Phys. D (Amsterdam, Neth.) **333**, 276 (2016).

[8] A. M. Kamchatnov and N. Pavloff, Phys. Rev. A **85**, 033603 (2012).

[9] J. J. Chang, P. Engels, and M. A. Hoefer, Phys. Rev. Lett. **101**, 170404 (2008).

[10] M. Marciante and M. S. Murillo, Phys. Rev. Lett. **118**, 025001 (2017).

[11] W. Lin, M. S. Murillo, and Y. Feng, Phys. Rev. E **100**, 043203 (2019).

[12] W. Lin, M. S. Murillo, and Y. Feng, Phys. Rev. E **101**, 013203 (2020).

[13] X. Ding, S. Lu, T. Sun, M. S. Murillo, and Y. Feng, Phys. Rev. E **103**, 013202 (2021).

[14] M. J. Ablowitz and D. E. Baldwin, Phys. Rev. E **87**, 022906 (2013).

[15] H. M. Thomas and G. E. Morfill, Nature (London) **379**, 806 (1996).

[16] L. I, W. T. Juan, C. H. Chiang, and J. H. Chu, Science **272**, 1626 (1996).

[17] A. Melzer, A. Homann, and A. Piel, Phys. Rev. E **53**, 2757 (1996).

[18] J. H. Chu and L. I, Phys. Rev. Lett. **72**, 4009 (1994).

[19] P. Hartmann, A. Z. Kovács, A. M. Douglass, J. C. Reyes, L. S. Matthews, and T. W. Hyde, Phys. Rev. Lett. **113**, 025002 (2014).

[20] R. Merlino and J. Goree, Phys. Today **57**, 32 (2004).

[21] E. Thomas Jr., U. Konopka, R. L. Merlino, and M. Rosenberg, Phys. Plasmas **23**, 055701 (2016).

[22] Y. Feng, J. Goree, and B. Liu, Phys. Rev. Lett. **100**, 205007 (2008).

[23] Y. Feng, J. Goree, and B. Liu, Phys. Rev. Lett. **109**, 185002 (2012).

[24] V. E. Fortov, A. V. Ivlev, S. A. Khrapak, A. G. Khrapak, and G. E. Morfill, Phys. Rep. **421**, 1 (2005).

[25] A. Piel, *Plasma Physics* (Springer, Heidelberg, 2010).

[26] G. E. Morfill and A. V. Ivlev, Rev. Mod. Phys. **81**, 1353 (2009).

[27] Y. Feng, J. Goree, and B. Liu, Phys. Rev. Lett. **104**, 165003 (2010).

[28] M. Bonitz, C. Henning, and D. Block, Rep. Prog. Phys. **73**, 066501 (2010).

[29] T. Ott, M. Stanley, and M. Bonitz, Phys. Plasmas **18**, 063701 (2011).

[30] Z. Haralson and J. Goree, Phys. Rev. Lett. **118**, 195001 (2017).

[31] T. Ott, M. Bonitz, and Z. Donkó, Phys. Rev. E **92**, 063105 (2015).

[32] A. Melzer, A. Schella, J. Schablinski, D. Block, and A. Piel, Phys. Rev. E **87**, 033107 (2013).

[33] Y. Feng, J. Goree, and B. Liu, Phys. Rev. Lett. **105**, 025002 (2010).

[34] P. Hartmann, A. Douglass, J. C. Reyes, L. S. Matthews, T. W. Hyde, A. Kovács, and Z. Donkó, Phys. Rev. Lett. **105**, 115004 (2010).

[35] M. S. Murillo, Phys. Plasmas **11**, 2964 (2004).

[36] A. Melzer, A. Schella, J. Schablinski, D. Block, and A. Piel, Phys. Rev. Lett. **108**, 225001 (2012).

[37] K. Qiao, J. Kong, J. Carmona-Reyes, L. S. Matthews, and T. W. Hyde, Phys. Rev. E **90**, 033109 (2014).

[38] B. Liu, J. Goree, V. Nosenko, and L. Boufendi, Phys. Plasmas **10**, 9 (2003).

[39] H. Yukawa, Proc. Phys.-Math. Soc. Jpn. **17**, 48 (1935).

[40] U. Konopka, G. E. Morfill, and L. Ratke, Phys. Rev. Lett. **84**, 891 (2000).

[41] Z. Donkó, G. J. Kalman, and P. Hartmann, J. Phys.: Condens. Matter **20**, 413101 (2008).

[42] Y. Feng, J. Goree, B. Liu, T. P. Intrator, and M. S. Murillo, Phys. Rev. E **90**, 013105 (2014).

[43] P. K. Shukla and A. A. Mamun, *Introduction to Dusty Plasma Physics* (Institute of Physics, Bristol, 2002).

[44] D. Samsonov, J. Goree, H. M. Thomas, and G. E. Morfill, Phys. Rev. E **61**, 5557 (2000).

[45] D. Samsonov, S. K. Zhdanov, R. A. Quinn, S. I. Popel, and G. E. Morfill, Phys. Rev. Lett. **92**, 255004 (2004).

[46] A. Kananovich and J. Goree, Phys. Rev. E **101**, 043211 (2020).

[47] T. Sun, M. S. Murillo, and Y. Feng, Phys. Plasmas **28**, 103703 (2021).

[48] T. Sun and Y. Feng, Phys. Plasmas **28**, 063702 (2021).

[49] J. Shen, S. Lu, T. Sun, and Y. Feng, Phys. Plasmas **29**, 053701 (2022).

[50] P. Qiu, T. Sun, and Y. Feng, Phys. Plasmas **28**, 113702 (2021).

[51] D. Samsonov, G. Morfill, H. Thomas, T. Hagl, H. Rothermel, V. Fortov, A. Lipaev, V. Molotkov, A. Nefedov, O. Petrov, A. Ivanov, and S. Krikalev, Phys. Rev. E **67**, 036404 (2003).

[52] See http://lammps.sandia.gov for the Simulation Software LAMMPS.

[53] G. J. Kalman, P. Hartmann, Z. Donkó, and M. Rosenberg, Phys. Rev. Lett. **92**, 065001 (2004).

[54] Y. Feng, B. Liu, and J. Goree, Phys. Rev. E **78**, 026415 (2008).

[55] G. A. El and M. A. Hoefer, Phys. D (Amsterdam, Neth.) **333**, 11 (2016).

[56] P. Hartmann, G. J. Kalman, Z. Donkó, and K. Kutasi, Phys. Rev. E **72**, 026409 (2005).

[57] G. A. El, M. A. Hoefer, and M. Shearer, SIAM Rev. **59**, 3 (2017).

[58] A. M. Kamchatnov, Phys. D (Amsterdam, Neth.) **333**, 99 (2016).